Tailoring the Local Interaction between Graphene Layers in Graphite at the Atomic Scale and Above Using Scanning Tunneling Microscopy

Hong Seng Wong,[†] Colm Durkan,[†,*] and Natarajan Chandrasekhar[‡]

[†]Nanoscience Centre, University of Cambridge, 11 JJ Thomson Avenue, Cambridge CB3 0FF, U.K., and [‡]Institute of Materials Research and Engineering, 3 Research Link, Singapore 117602

ABSTRACT With recent developments in carbon-based electronics, it is imperative to understand the interplay between the morphology and electronic structure in graphene and graphite. We demonstrate controlled and repeatable vertical displacement of the top graphene layer from the substrate mediated by the scanning tunneling microscopy (STM) tip−sample interaction, manifested at the atomic level as well as over superlattices spanning several tens of nanometers. Besides the full-displacement, we observed the first half-displacement of the surface graphene layer, confirming that a reduced coupling rather than a change in lateral layer stacking is responsible for the triangular/honeycomb atomic lattice transition phenomenon, clearing the controversy surrounding it. Furthermore, an atomic scale mechanical stress at a grain boundary in graphite, resulting in the localization of states near the Fermi energy, is revealed through voltage-dependent imaging. A method of producing graphene nanoribbons based on the manipulation capabilities of the STM is also implemented.

KEYWORDS: graphene · STM · HOPG · surface

Given the different ways in which carbon atoms can bond to each other to produce diamond, graphene, nanotubes, and fullerenes, as well as a host of related materials, there is understandably a high level of interest in manufacturing electronic devices based on carbon.[1,2] Given their cost, nonspecificity, and now their toxicity, the dream of using carbon nanotubes in device structures is rapidly receding. This is, however, being replaced by graphene, which possesses a variety of intriguing electronic and mechanical properties—this is manifested as band structure and film morphology, which vary with the number of layers, and can hence be tuned locally.[3] However, as we will see, there are many useful lessons still to be learned from looking at graphite, which we report on in this article. Graphite is composed of layers of sp^2-bonded carbon atoms arranged in a honeycomb lattice, Bernal stacked along the *c*-axis, bonded by weak van der Waals forces. It has been used as a standard substrate in STM experiments for over 25 years, and its structure, both morphological and electronic, is reasonably well-understood both theoretically and experimentally. Despite the correlation of electronic density of surface states with the surface geometric topography for most substrates, graphite nevertheless exhibits some intriguing phenomena. One such phenomenon is the difficulty in obtaining a true view of the honeycomb atomic structure by STM due to the electronic interaction between the surface graphene layer and the underlying layers. Calculations have predicted a lower electronic density of states (DOS) at the Fermi level for carbon atoms that are situated directly above a carbon atom in the underlying layer (α-atoms) relative to carbon atoms that are not (β-atoms).[4,5] This is due to π-states localized above alternate carbon−carbon bonds.[6] Therefore, the typical atomic resolution image of graphite imaged by STM shows a triangular lattice, with a hexagonal symmetry modulation of 0.246 nm periodicity, as compared to 0.142 nm between adjacent carbon atoms. Nevertheless, there have been numerous reports on the observation of the honeycomb atomic lattice by STM, assigning them to either a tip modification which increases the number of occupied orbitals probed at the Fermi level,[6−8] reduced mechanical tip−sample interaction,[9] or the displacement of the top graphene layer.[10−13] Such controversy arises because the triangular/honeycomb transition phenomenon is imaged as an abrupt transition from one linescan to the next, as shown in Figure 1a, which is exactly what happens when the tip state changes. Even within the displacement explanation, there

*Address correspondence to cd229@eng.cam.ac.uk.

Received for review July 27, 2009 and accepted September 23, 2009.

Published online October 1, 2009.
10.1021/nn9011785 CCC: $40.75

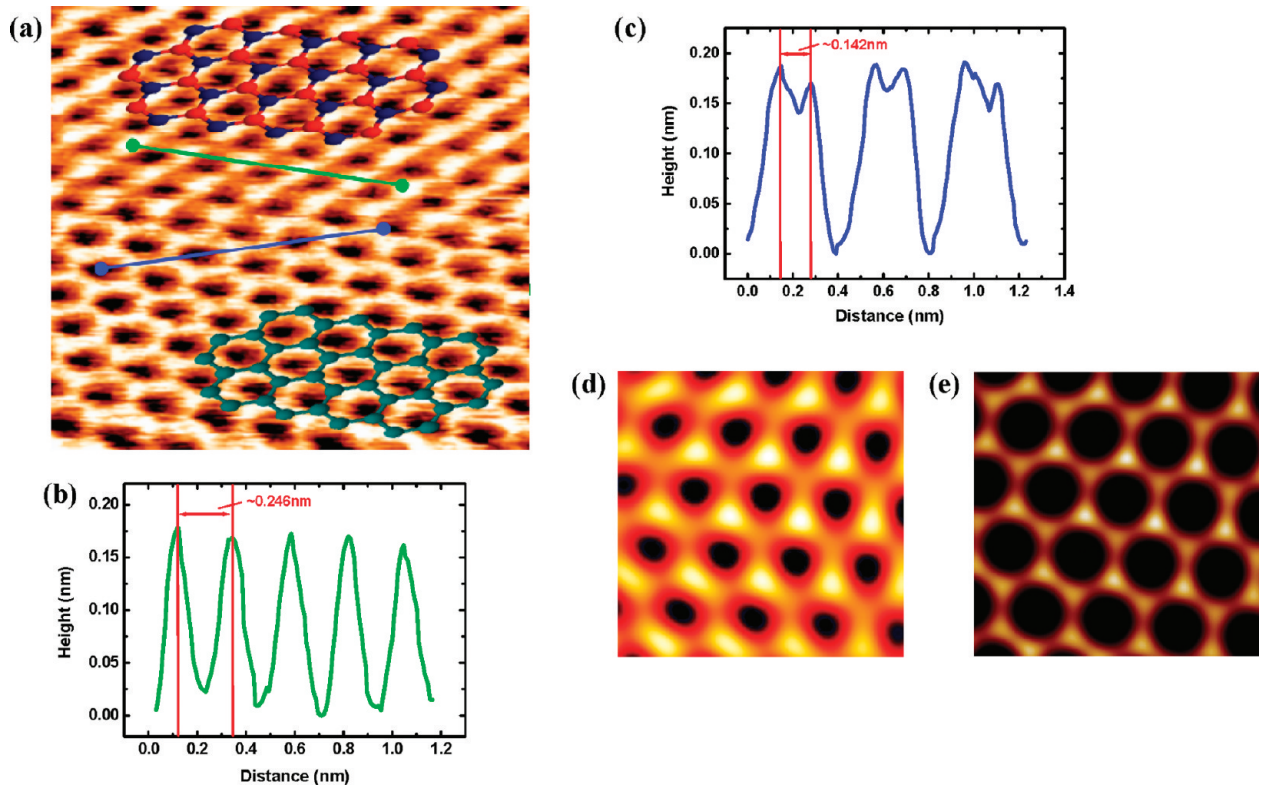

Figure 1. (a) Atomic resolution of bare graphite showing coexistence of the triangular and honeycomb lattice (0.1 V, 0.40 nA) with the atomic model fitted (2 × 2 nm^2). The bottom half of the image where the honeycomb traverses across the entire length of the linescan is termed "full-displacement". (b) Line profile along triangular lattice showing the distance between every other atom. (c) Line profile along honeycomb lattice revealing two pronounced maxima corresponding to two adjacent carbon atoms measured to be 0.142 nm. (d,e) Density of states simulation of graphite triangular and honeycomb STM images under normal coupling and 20% of normal coupling, respectively, using A−B stacking for both instances (1 × 1 nm^2 area).

is no common ground, but speculations regarding a change in stacking from A−B to A−A are ubiquitous since, in the A−A configuration, each surface atom interacts equally with the underlying layer and should possess an equal density of states. STM observations on graphene on an insulator are consistent with this explanation, as monolayer and bilayer films display honeycomb and triangular lattices, respectively.[14] Observations of epitaxially grown graphene on a metal substrate further illustrated the complexity of interlayer interactions in determining the apparent atomic arrangement.[15] The question to answer is thus: What is the true origin of this triangular/honeycomb transition? And if displacement indeed occurs, what is the true mechanism behind it? The honeycomb images reported so far extend along the whole length of the linescan, which we term as "full-displacement".

The extremely low sliding friction between graphene layers of which graphite is composed makes it an extremely good lubricant and, together with its relatively high abundance, makes graphite ideal for use as pencil lead. One consequence, however, of this low friction is that the layers on graphite may easily be laterally misoriented with respect to each other. This manifests itself electronically as a superperiodic interference structure: a *superlattice*, with periods typically in the range of 1−10 nm, akin to the optical interference patterns typically associated with Moiré interference,[12,16−21] although there are other explanations which fit a small number of experiments as well such as tip-induced surface deformation,[4,22] multiple tip effects,[23] and dislocation networks.[24] Observations of graphite superlattices by STM are commonplace, albeit random, and without any application to date since their electronic properties are assumed to be inalterable or at least appear so. However, given the weak electronic coupling between the layers of graphene in graphite, studies of superlattices can be used to gain a better understanding of how graphene sheets will interact with a given substrate. These superstructures are, of course, not unique to graphite and graphene and have also been observed in multiwalled carbon nanotubes, where the Moiré explanation was found to hold also.[25]

In this work, we use the signature of a superlattice to ascertain the true origin of the triangular/honeycomb atomic lattice transition and have extended this to demonstrate displacement over lateral length scales of several tens of nanometers. Our results present the first direct evidence which answer the longstanding controversy as to the origin and mechanism behind the triangular/honeycomb atomic transition as well as the origin of superlattices. We have also used the presence of a superlattice to investigate surface strain at the atomic scale, heralding a novel method for materials

characterization and pave the way in engineering the electronic properties by introducing an atomic scale stress. The article is then concluded by implementing a method for producing graphene nanoribbons through STM manipulation. Besides advocating the application of superlattices in carbon electronics, this article explores the various capabilities and functionalities of STM in terms of its imaging, spectroscopic and manipulation techniques at room temperature.

RESULTS AND DISCUSSION

The Honeycomb Atomic Lattice. Figure 1a shows an atomic resolution image of bare graphite in the vicinity of a superlattice and a defect (in this case, a grain boundary). A transition from triangular to honeycomb lattice is clearly observed during scanning. This is relatively commonplace in STM imaging and is typically ascribed to a random tip change. We will show, however, this is not always the case and is, in fact, highly reproducible.

We have used a simple analytical model describing the spatial variation of the density of states of graphite, which we reported previously.[26] In this model, STM images are simulated by considering the top three layers with relative weightings of 1, −0.5, and 0.125, where the variation in weighting is simply due to the distance of the layers from the tip and the minus sign for the second layer represents the fact that the stacking is A−B. These weightings have been found to give the best agreement with experimental STM images, and they apply when the distance between the layers is 0.335 nm (which we will refer to as *normal coupling*). Modification of the interlayer distance through the tip−sample interaction will result in a shift in these weightings and therefore a change in the image contrast, which is the essential finding reported in this article. It is also a simple matter to introduce a lateral rotation between the layers and produce a superlattice, whose periodicity is as expected from the Moiré pattern assumption.

The line profiles in Figure 1b,c further reveal the differences between the triangular and honeycomb lattices, which can be compared to simulations of the density of states of both as shown in Figure 1d,e, respectively. Since the honeycomb lattice traverses the entire linescan, we regard this as full-displacement. Within the displacement theory, there exist two traditionally accepted explanations: (i) the tip has laterally displaced the surface graphene sheet to change the stacking from A−B to A−A, which is extremely unlikely given the size of the sheet; or (ii) the tip has lifted the surface layer enough (*i.e.*, a few angstroms) to significantly reduce the coupling with the layer below. To verify this, simulations were done on the basis that, in Figure 1d, the stacking is A−B with the normal coupling between the layers, whereas in Figure 1e, it is still A−B but the surface layer has been lifted to reduce the coupling with the second and third layers to 20% of the normal value. At around this point, the honeycomb lattice becomes noticeable. Given that the coupling between layers separated by a distance d (in nm) is $e^{-0.24d}$,[17] we find that the additional displacement induced by the STM tip is of the order 3.3 Å (*i.e.*, the distance between the displaced top layer and the layer underneath is 6.7 Å), which is coincidentally rather close to the interlayer spacing in graphite. As such, we propose that a reduced coupling rather than a stacking change is pivotal in the transition between the two observed atomic structures. This will be further validated and elucidated in the later part of this article, where we furthermore observe a similar transition over a much larger lateral scale as well as a "half-displacement".

Manifestation of Atomic Scale Strain and Surface Displacement. To demonstrate the role of superlattices' signature in identifying surface displacement and atomic scale strain, we must first locate and characterize a superlattice. Figure 2a shows conjoined superlattices, each with a different corrugation, periodicity, and orientation. It is clear from this image (and Figure 2d) that the surface layer is continuous. Therefore, we propose that the boundary between these two sets of superlattices coincides with a grain boundary in the layer(s) underneath, where each grain has a slightly different orientation. For the superlattice on the left (which we will henceforth refer to as the left superlattice), besides having a lower corrugation than the one on the right (Figure 2c), there is a gradient in the periodicity, indicating that the grain boundary underneath is low angle, consisting of a series of screw dislocations. The lower region has a periodicity of 7.1 nm, decreasing gradually toward the upper region, where the periodicity is 6.5 nm. The implication of this is that the misorientation angle between the surface and underlying graphene layers will be smaller on the lower region because the longer the periodicity, the higher the misorientation angle, according to the Moiré model. As the periodicity of 5.9 nm in the superlattice on the right (which we will henceforth refer to as the right superlattice) is constant throughout, the atomic lattice misorientation angle of the underlying layer between the two regions of superlattices will be greater at the lower region.

In calculating the rotational misorientation between two graphene layers, we employ the Moiré pattern formula: The periodicity, D, of the resulting Moiré superperiodic hexagonal structure is related to the rotation angle, θ, between the two layers of the hexagonal lattice, with lattice constant d, as $D = d/[2 \sin(\theta/2)]$.[19] The orientation of the Moiré pattern, $\square$, with respect to the atomic orientation of the top layer is related to the rotation angle, θ, as $\square = 30° - (\theta/2)$. The calculated rotational angle between the two graphene layers, from the measured superlattice periodicity of 5.9 nm, is 2.39°.

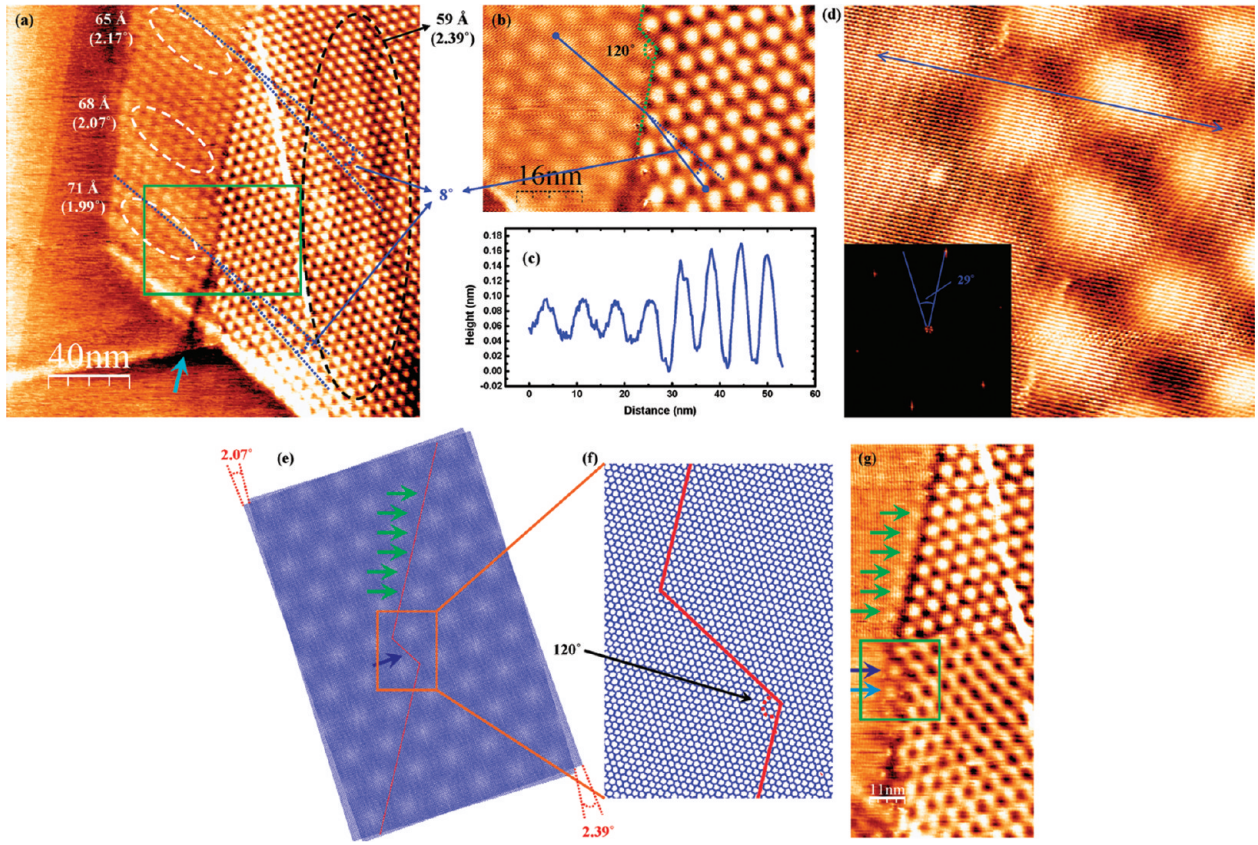

Figure 2. (a) Two sets of superlattices showing a region of higher contrast (right) and a region of lower contrast (left) (−0.3 V, 0.2 nA). Superlattice periodicities at different regions are indicated with the calculated misorientation angle (as bracketed). Light blue arrow indicates where the fault/boundary begins. Angular mismatch between the two sets of superlattice is 8°. Linear ripples indicated by the black dotted ellipse on the right superlattice demonstrate buckling. (b) Region indicated by a green box in (a) having a change in the fault direction of 120° (−0.3 V, 0.2 nA). (c) Line profile across the boundary as depicted by the solid blue line in (b). All periodicities are measured from an average of at least four superlattice corrugations. (d) A 20 × 20 nm² area at the boundary between the right and left superlattices with atomic resolution (0.05 V, 0.2 nA), Bottom left inset: FFT of the right superlattice. Outer hexagonal spots correspond to the atomic lattice, while the inner hexagonal spots correspond to the superlattice. The blue line, which traverses the boundary, shows no atomic mismatch between both regions, indicating that the surface graphene layer for both regions is continuous. The misorientation angle between the superlattice and atomic lattice is 29°, measured from the FFT. (e) Proposed Moiré rotational pattern model with the fault/boundary line in red. Green and blue arrows show the locations where compressive stresses are present at the boundary caused by a difference in the misorientation angle at both regions which results in a slight difference in superlattice periodicity in both regions as shown (a). (f) Proposed fault/boundary line having a 120° directional change indicates that the fault will result in terminations with armchair edges. (g) Boundary imaged at −0.1 V showing locations with enhanced density of states due to the localization of states induced near the Fermi energy attributed to stresses as indicated in (e) (0.2 nA).

The calculated misorientation angle for the Moiré pattern will then be 28.81°, which agrees well with the measured value of 29° from the FFT (fast Fourier transform) in Figure 2d, validating the Moiré rotation assumption.

A model of the grain boundary in the underlying graphene sheets is depicted in Figure 2e, in accordance with Figure 2b. Due to the misorientation between the grains, we would expect that the boundary will result in atomic scale compressive stresses being exerted in some regions along the boundary as indicated. It is known that the presence of local stresses induces localization of states near the Fermi energy.[27,28] Upon imaging at −0.1 V, the enhanced density of states becomes apparent at the locations indicated by the arrows in Figure 2g, corresponding to those indicated in the model (Figure 2e). The stress exerted decreases from the lower region to the upper region due to the smaller atomic misorientation angle in the upper region. Therefore, localization of states is expected predominantly in the lower region. Closer inspection of Figure 2a reveals that the surface layer on the right superlattice region is buckled, as indicated by the linear ripples in the region of the image in the black dotted ellipse drawn. These ripples are not parallel to the boundary but to the nanoribbon (Figure 4) close to the boundary and shows that the surface layer is more easily deformable on the right superlattice region than on the left. Furthermore, in Figure 2g, there is a transition in the appearance of the superlattice about halfway up the image. We attribute this to a large-scale vertical displacement of the surface layer, which will be discussed in detail later. Knowing the angle of the boundary as well as the atomic orientation of the underlying graphene sheet (from the atomic orientation of the surface layer and the calculated misorientation angle), we

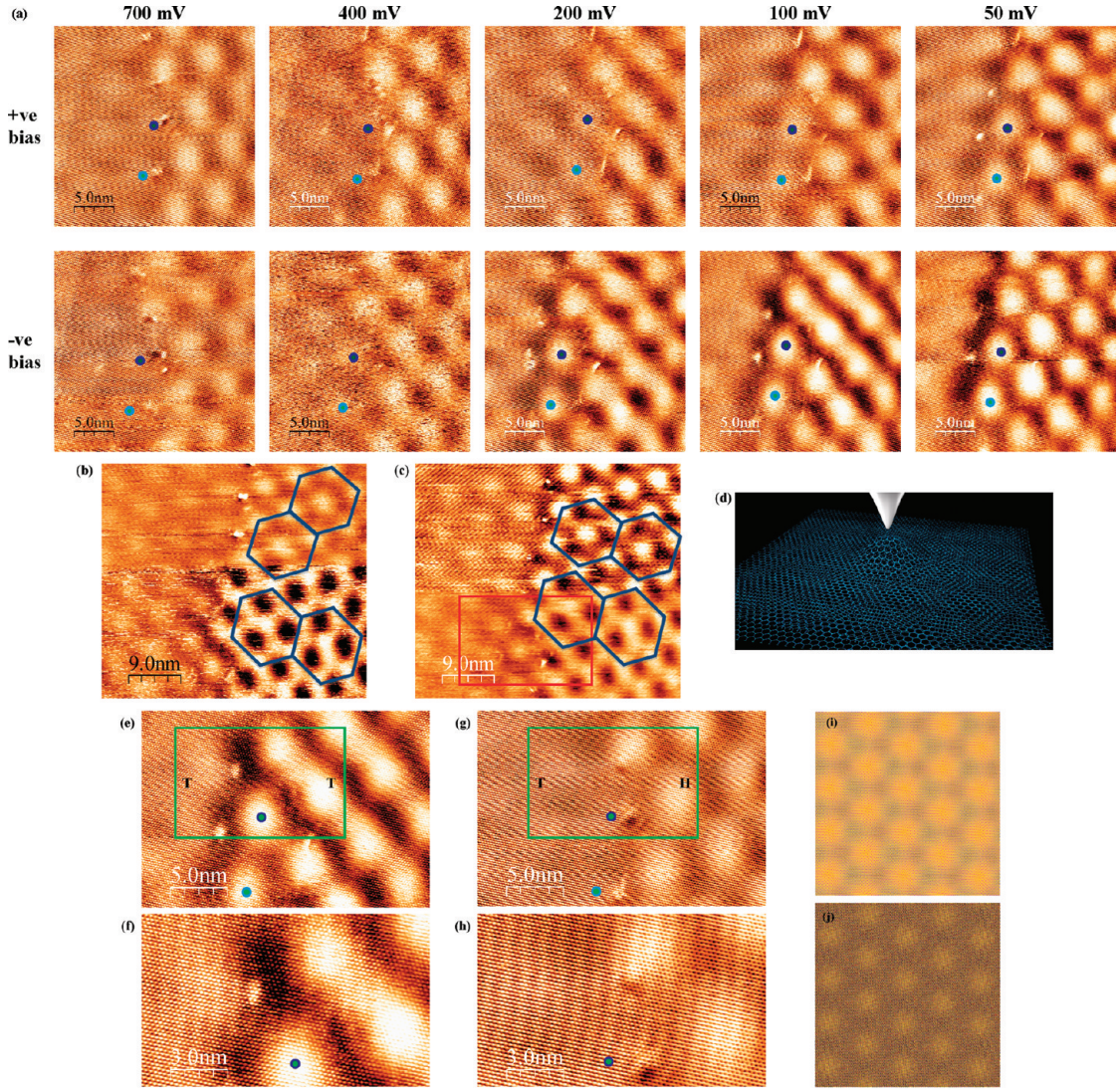

Figure 3. (a) Voltage-dependent STM imaging of the same region indicated by a green box in Figure 2g (0.2 nA). As the bias magnitude decreases (*i.e.*, probing levels near the Fermi energy), the contrast at the blue dots increases, demonstrating the presence of localized states near the Fermi level induced by a local stress. The darker blue dot has a slightly higher contrast since it is directly next to the 120° bend in the fault line, as indicated by the blue arrow in Figure 2e,g and therefore experiences a higher stress. (b) Transition in superlattice contrast due to lifting and "dropping" of the surface graphene layer, when imaged at 0.7 V and (c) −0.3 V, 0.2 nA. Note the stretching of the hexagonal superlattice unit cell by 16% upon surface displacement in both conditions. (d) Illustration of the warping and displacement of the top graphene layer induced by the tip, which causes the superlattice stretching and a change in contrast. Superlattice pattern is also observed in this illustration caused by the rotational mismatch of the two graphene layers. (e−h) Zoom-ins of the boundary indicated by a red box in (c) imaged at (e) −0.1 V, 0.2 nA and (g) 0.5 V, 0.2 nA. (f,h) Respective magnified region indicated by a green box. Transition from triangular (T) to honeycomb (H) atomic lattice is clearly discernible in (h), while no transition is observed in (f). Note that, under both conditions, the left region shows a triangular atomic lattice, implying a constant surface coupling with the underlying layer. The change in atomic structure occurs only on the right region (half-displacement), demonstrating the ease of surface displacement on the right region where the superlattice corrugation is higher (and is reduced during displacement), and confirms the displacement theory and reduced coupling hypothesis. Blue dots indicate the region of stress as discussed in (a). Simulation of superlattice with 2.39° of orientation mismatch between the top and subsequent layers for (i) normal coupling and (j) 20% of normal coupling between the layers. Both images are 25 nm × 25 nm. From the image, it is clear that the superlattice orientation is unaltered with reduced coupling, the main difference being that the contrast is significantly reduced. There is a more dramatic difference at the atomic scale where the reduced coupling causes a transition between the triangular and atomic lattice structures, as shown in Figure 1 and (e)−(h).

can extract the termination structure of the proposed fault line using a simple atomic model as shown in Figure 2f. From our analysis, we predict that the fracture along the fault line will produce terminations with armchair edges.

From Figure 2g, it appears that there is a relatively larger stress being exerted in the region where the fault line changes direction at an angle of 120°, as indicated by the dark blue arrow. As such, we performed voltage-dependent imaging in the area indicated by the green

box to probe for the presence of localized states. From Figure 3a, it is evident that a decrease in the magnitude of the applied voltage (*i.e.*, imaging closer to the Fermi energy) reveals an increase in the density of states in the region indicated by the blue dots for both polarities. There is a small asymmetry in the electronic states, with larger density of additional states below the Fermi energy as compared to above it. Superlattices have always been shown to be a superperiodic interference pattern with an enhanced density of states, but our result indicates that this electronic state could be further enhanced locally through the application of stress. In addition, the location directly below the fault line experiences the most stress, as indicated by the darker blue dot (slightly higher DOS), as compared to a region a few nanometers away from the fault, as indicated by the lighter blue dot (slightly lower DOS). As such, the graphite superlattice could well serve as a means of mapping the nanoscale stress gradient in graphite even for stresses just beneath the surface.

In recent years, there has been a spate of research focusing on graphene edges,[29−31] both experimentally and theoretically, emphasizing the difference in the density of states between zigzag and armchair-terminated edges. Zigzag-terminated ribbons possess a unique filled edge state close to the Fermi level, stemming from the topology of its π-electron networks, which is not present in armchair ribbons. In our case, it is unlikely that the localization of states is caused by the presence of zigzag edges since the termination consists mainly of armchair edges as discussed earlier. We find that the localization of states occurs gradually with decreasing bias for both polarities of sample voltage, albeit with a slight asymmetry toward there being more filled states, all indicating that our assertion of local compressive stress is valid.

After performing several scans in the boundary region, we observe the occurrence of a transition in the superlattice structure (Figure 3b,c), which we attribute to the decoupling of the surface layer relative to underlying layers, analogous to what is shown in Figure 1a for the atomic lattice. In fact, after the transition, the atomic lattice switches from triangular to honeycomb. In all cases, the orientation and position of the superlattice remain unchanged after surface decoupling, but the symmetry becomes distorted, corresponding to stretching of the superlattice unit cell by 16% in the y-direction, as shown by the inserted honeycomb model (Figure 3b,c). This shows that the transition is not simply a switch in the image contrast due to a change in the tip state. Also, the transition cannot be explained as a lateral shift of the surface layer modifying the stacking from A−B to A−A, as this shift at the atomic scale would result in a significant shift of the superlattice peak positions, which we do not observe. The occurrence of the transition is independent of the voltage. This implies a weak interaction between the surface and the underlying layer especially in the right superlattice region, such that even at an increased tip−sample distance (associated with a bias of 0.7 V) decoupling of the surface graphene sheet still occurs. We propose that this is made possible here due to the tapered shape of the surface layer in the scan area, meaning it is relatively easy to be lifted by the tip. The higher superlattice corrugation could also enhance the surface deformation. It has been shown that the corrugation of superlattices decreases with increasing voltage as the interlayer influence is only important near the Fermi level[18,32] and decreases with decreasing current (*i.e.*, increasing tip−surface distance).[20] Nonetheless, it is evident that the corrugation of the portion of superlattice that has been displaced in the lower half of Figure 3b (2 Å) at a sample bias of 0.7 V is significantly larger than at the lower bias of −0.3 V in Figure 3c (0.5 Å). This is due to a consequent increase in the average tip−sample distance after surface decoupling. In Figure 3d, we have illustrated the warping of the surface graphene layer under the STM tip.

The decoupling of the surface graphene sheet induced by an STM tip is already known and, in fact, is the reason for the observed anomalous atomic corrugation of graphite on the order of 0.1−0.2 nm, which is ultimately the reason for its common use in STM experiments. The scanning tip is in extreme close proximity to the graphite surface during tunneling because graphite is a semimetal with a low density of states. This results in a large attractive tip−surface interaction leading to surface deformation[4,22] and displacement.[12,21,33,34] The already weak interlayer coupling in graphite would be further reduced by the presence of any intrinsic defects. Since our experiments were carried out directly on a superlattice, which implies an intrinsic underlying defect, and in the vicinity of a grain boundary, this region would have a much weaker interlayer coupling. Therefore, the surface graphene layer will be prone to decoupling by the STM tip−sample interaction during tunneling. Finally, the lateral scan speed of the tip used in our experiment is relatively high (2 Hz for all scan sizes). An increased scan speed decreases the effectiveness of the feedback mechanism of the STM, thus allowing the tip to get closer to the surface and increase the likelihood of decoupling the surface layer. An increase in scanning speed has previously been reported to enhance the likelihood of surface displacement.[11]

From Figure 3b,c, we know that surface displacement occurs only on the right superlattice region, implying a weaker coupling as compared to the left superlattice region. To further validate this point and rebut the tip state modification explanation for observation of superlattices and the honeycomb atomic lattice, we imaged the boundary area indicated by a red box in Figure 3c, where the transition occurs for the right superlattice. Atomic resolution images of graphite are obtained for both regions in the same image plane as shown in Figure 3e,g. Panels f and h of Figure 3 are their respective magnified areas for clarity. Figure 3h shows a transition in the atomic lattice from triangular to honeycomb when traversing

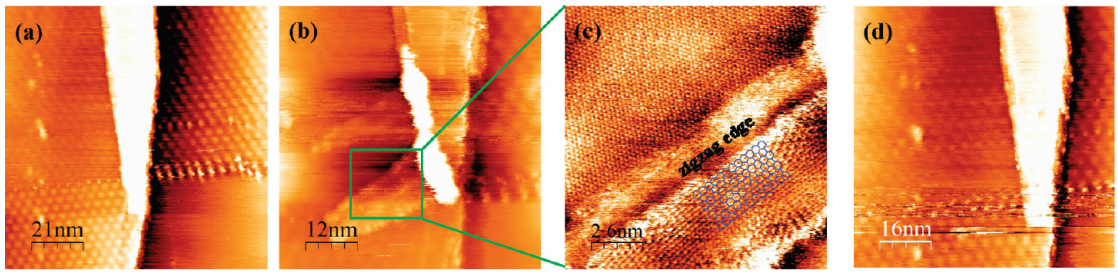

Figure 4. (a) Graphite flake on a step in the vicinity of a grain boundary, resulting in a superlattice (0.4 V, 0.2 nA). (b) Modified step after STM tip has been used to peel back flake, resulting in a bilayer graphene nanoribbon (0.4 V, 0.2 nA). (c) Zoom-in on the nanoribbon reveal complex pattern where the orientation of atomic rows indicates a zigzag edge termination (0.4 V, 0.2 nA). (d) Nanoribbon has been refolded back to its original position (0.5 V, 0.2 nA).

across the boundary (from left to right), while no transition is observed in Figure 3f (the atomic lattices for both regions remain triangular). We termed this phenomenon half-displacement because the displacement occurs from the middle of each linescan. The occurrence of this transition is again independent of the applied voltage and its polarity. Note that the atomic lattice on the left superlattice region remains triangular, which implies that the left region remains fully coupled at all times and only the right region experiences a series of both coupling and decoupling phenomena under different scanning instances. This observation is a direct evidence of decoupling, consistent with the displacement hypothesis because the higher superlattice corrugation means that the elastic deformation over that region is stronger. In addition, knowing that the surface layer between the two regions is continuous, strongly supports the simulation in Figure 1e that the half-displacement is caused by reduced coupling rather than a change in the stacking from A−B to A−A since such stacking change will certainly result in both regions having the same atomic structure, which is not the case. As such, the message which both panels f and h of Figure 3 (the half-displacement) deliver is consequential. Besides affording a cogent evident that a displacement indeed occurs, it also confirms the type of displacement taking place. This is further highlighted in Figures 1d,e and 3i,j, where we present simulations of the density of states of the surface. In Figure 1d,e, we show that, under normal coupling, the triangular lattice is observed, whereas under reduced coupling (20%), the pattern at the atomic scale is a hybrid triangular−honeycomb structure, which the STM observes as a honeycomb structure. In Figure 3i,j, which shows simulations over larger areas (25 nm), we show that a superlattice is still observed in both cases, albeit with a greatly reduced contrast in the case of reduced coupling, as expected, and consistent with our experiments.

Producing Graphene Nanoribbon through STM Manipulation. The capability of the STM to manipulate atoms and molecules is already well-established,[35,36] but the application to larger structures is still in its infancy especially at room temperature. We have demonstrated here that, while imaging HOPG, the sample warps under the tip, and the scanning conditions can be optimized to allow the top graphene layer to be decoupled from the underlying layers by a few angstroms. The next step, of course, is to perform this with more control to ultimately fabricate a device whose electrical characteristics can be modulated by the presence of a superlattice. The first step toward this is illustrated in Figure 4, where we have used the STM tip to fold over the edge of the top few layers of graphene (Figure 4b) with zigzag terminations on HOPG, followed by a successful manipulation back to the original configuration (Figure 4d). The resulting superstructure, due to the misorientation between the layers, is clearly visible (Figure 4c). Through suitable manipulation pathways and selection of folding regions, it is possible to control the superlattice periodicity, along with the desired graphene size and edge termination. This should alter the electronic band structure and introduce sub-bands, whose electrical characteristics can be utilized in a novel few layers graphene device structure, thus enhancing carbon electronics.

To conclude, we have shown that by studying the properties of HOPG carefully, we can learn something useful for future graphene electronics as well as for general STM imaging and manipulation. We have mapped local strain in the vicinity of a defect through voltage dependent imaging of superlattices and have successfully used STM to manipulate and alter the coupling between individual graphene sheets. This further extends the evidence that studies on graphene, if they are not free-standing films, must be taken with great caution due to the coupling with any substrate.

METHODS

All STM images were acquired at constant current with an Omicron UHV STM/AFM system at room temperature. Mechanically cut Pt/Ir tips were used. HOPG substrates were prepared by cleaving with tape and treated with 1,2,4-trichlorobenzene to induce the formation of superlattices.[13] The sample was then introduced into a load-lock chamber and pumped down overnight to a pressure in the order of 10^{-10} mbar prior to scanning. There

is no evidence of intercalation of the solvent, as atomic resolution imaging of different areas around the superlattices reveals that the measured atomic misorientation between layers is consistent with that expected from the superlattice periodicity based on the Moiré pattern assumption. All STM images presented here were processed using WSxM[37] without smoothing. Simulations of STM images of the honeycomb and triangular lattice were done using the model for density of states as reported in ref 26. For the results shown in Figure 4, the original image was taken with a bias voltage of 0.4 V and a scan rate of 1.5 Hz, and for the manipulation, this was altered to 0.1 V and 2 Hz. To manipulate the flake back, the bias voltage was again reduced to 0.1 V.

Acknowledgment. We acknowledge Ms. Yun-Thai Li for the graphene illustration in Figure 3d. We also acknowledge funding support from the EPSRC spinmol project. H.S.W. thanks Astar (Singapore) for funding his studies.

REFERENCES AND NOTES

1. Avouris, P.; Chen, Z.; Perebeinos, V. Carbon-Based Electronics. *Nat. Nano* **2007**, *2*, 605–615.
2. Geim, A. K.; Novoselov, K. S. The Rise of Graphene. *Nat. Mater.* **2007**, *6*, 183–191.
3. Kim, D.-H.; Rogers, J. A. Bend, Buckle, and Fold: Mechanical Engineering with Nanomembranes. *ACS Nano* **2009**, *3*, 498–501.
4. Batra, I. P.; García, N.; Rohrer, H.; Salemink, H.; Stoll, E.; Ciraci, S. A Study of Graphite Surface with STM and Electronic Structure Calculations. *Surf. Sci.* **1987**, *181*, 126–138.
5. Tománek, D.; Louie, S. G. First-Principles Calculation of Highly Asymmetric Structure in Scanning-Tunneling-Microscopy Images of Graphite. *Phys. Rev. B* **1988**, *37*, 8327.
6. Zeinalipour-Yazdi, C. D.; Pullman, D. P. A New Interpretation of the Scanning Tunneling Microscope Image of Graphite. *Chem. Phys.* **2008**, *348*, 233–236.
7. Moriarty, P.; Hughes, G. Atomic Resolved Material Displacement on Graphite Surfaces by Scanning Tunnelling Microscopy. *Appl. Phys. Lett.* **1992**, *60*, 2338.
8. Mizes, H. A.; Park, S.-i.; Harrison, W. A. Multiple-Tip Interpretation of Anomalous Scanning-Tunnelling-Microscopy Images of Layered Materials. *Phys. Rev. B* **1987**, *36*, 4491–4494.
9. Atamny, F.; Spillecke, O.; Schlögl, R. On the STM Imaging Contrast of Graphite: Towards a "True" Atomic Resolution. *Phys. Chem. Chem. Phys.* **1999**, *1*, 4113–4118.
10. Ouseph, P. J.; Poothackanal, T.; Mathew, G. Honeycomb and Other Anomalous Surface Pictures of Graphite. *Phys. Lett. A* **1995**, *205*, 65.
11. Paredes, J. I.; Martinez-Alonso, A.; Tascon, J. M. D. Triangular Versus Honeycomb Structure in Atomic-Resolution STM Images of Graphite. *Carbon* **2001**, *39*, 476.
12. Luican, A.; Li, G.; Andrei, E. Y. Scanning Tunneling Microscopy and Spectroscopy of Graphene Layers on Graphite. *Solid State Commun.* **2009**, *149*, 27–28.
13. Wang, Y.; Ye, Y.; Wu, K. Simultaneous Observation of the Triangular and Honeycomb Structures on Highly Oriented Pyrolytic Graphite at Room Temperature: An STM Study. *Surf. Sci.* **2006**, *600*, 729.
14. Stolyarova, E.; Rim, K. T.; Ryu, S.; Maultzsch, J.; Kim, P.; Brus, L. E.; Heinz, T. F.; Hybertsen, M. S.; Flynn, G. W. High-Resolution Scanning Tunneling Microscopy Imaging of Mesoscopic Graphene Sheets on an Insulating Surface. *Proc. Natl. Acad. Sci. U.S.A.* **2007**, *104*, 9209.
15. Sutter, E.; Acharya, D. P.; Sadowski, J. T.; Sutter, P. Scanning Tunneling Microscopy on Epitaxial Bilayer Graphene on Ruthenium (0001). *Appl. Phys. Lett.* **2009**, *94*, 133101.
16. Varchon, F.; Mallet, P.; Magaud, L.; Veuillen, J.-Y. Rotational Disorder in Few-Layer Graphene Films on 6*H*-SiC(000−1): A Scanning Tunnelling Microscopy Study. *Phys. Rev. B* **2008**, *77*, 165415.
17. Pong, W. T.; Durkan, C. A Review and Outlook for an Anomaly of Scanning Tunnelling Microscopy (STM): Superlattices On Graphite. *J. Phys. D: Appl. Phys.* **2005**, *38*, R329–R355.
18. Rong, Z. Y.; Kuiper, P. Electronic Effects in Scanning Tunneling Microscopy: Moiré Pattern on a Graphite Surface. *Phys. Rev. B* **1993**, *48*, 17427.
19. Kuwabara, M.; Clarke, D. R.; Smith, D. A. Anomalous Superperiodicity in Scanning Tunneling Microscope Images Of Graphite. *Appl. Phys. Lett.* **1990**, *56*, 2396.
20. Osing, J.; Shvets, I. V. Bulk Defects in Graphite Observed with a Scanning Tunnelling Microscope. *Surf. Sci.* **1998**, *417*, 145–150.
21. Bernhardt, T. M.; Kaiser, B.; Rademann, K. Formation of Superperiodic Patterns on Highly Oriented Pyrolytic Graphite by Manipulation of Nanosized Graphite Sheets with the STM Tip. *Surf. Sci.* **1998**, *408*, 86–94.
22. Soler, J. M.; Baro, A. M.; Garcia, N.; Rohrer, H. Interatomic Forces in Scanning Tunneling Microscopy: Giant Corrugations of the Graphite Surface. *Phys. Rev. Lett.* **1986**, *57*, 444.
23. Albrecht, T. R.; Mizes, H. A.; Nogami, J.; Park, S.-il.; Quate, C. F. Observation of Tilt Boundaries in Graphite by Scanning Tunneling Microscopy and Associated Multiple Tip Effects. *Appl. Phys. Lett.* **1988**, *52*, 362–364.
24. Garbarz, J.; Lacaze, E.; Faivre, G.; Gauthier, S.; Schott, M. Dislocation Networks in Graphite: A Scanning Tunneling Microscopy Study. *Philos. Mag. A* **1992**, *65*, 853.
25. Tison, Y.; Giusca, C. E.; Sloan, J.; Silva, S. R. P. Registry-Induced Electronic Superstructure in Double-Walled Carbon Nanotubes, Associated with the Interaction between Two Graphene-like Monolayers. *ACS Nano* **2008**, *2*, 2113.
26. Pong, W. T.; Durkan, C. Simple Model of Electronic Density of States of Graphite and Its Application to the Investigation of Superlattices. *J. Appl. Phys., Part 1* **2005**, *44*, 5365–5369.
27. Kılıç, Ç.; Mehrez, H.; Ciraci, S. Quantum Point Contact on Graphite Surface. *Phys. Rev. B* **1998**, *58*, 7872–7881.
28. Owen, J. H. G.; Miki, K.; Bowler, D. R. Interaction between Electronic Structure and Strain in Bi Nanolines on Si(001). *Surf. Sci. Lett.* **2003**, *527*, L177–L183.
29. Enoki, T.; Kobayashi, Y.; Fukui, K. Electronic Structures of Graphene Edges and Nanographene. *Int. Rev. Phys. Chem.* **2007**, *26*, 609–645.
30. Ritter, K. A.; Lyding, J. W. The Influence of Edge Structure on the Electronic Properties of Graphene Quantum Dots and Nanoribbons. *Nat. Mater.* **2009**, *8*, 235.
31. Castro Neto, A. H.; Guinea, F.; Peres, N. M. R.; Novoselov, K. S.; Geim, A. K. The Electronic Properties of Graphene. *Rev. Mod. Phys.* **2009**, *81*, 109.
32. Charlier, J.-C.; Michenaud, J.-P.; Lambin, Ph. Tight-Binding Density of Electronic States of Pregraphitic Carbon. *Phys. Rev. B* **1992**, *46*, 4540.
33. Snyder, S. R.; Foecke, T.; White, H. S.; Gerberich, W. W. Imaging of Stacking Faults in Highly Oriented Pyrolytic Graphite Using Scanning Tunneling Microscopy. *J. Mater. Res.* **1992**, *7*, 341–344.
34. Pethica, J. B. Comment on "Interatomic Forces in Scanning Tunneling Microscopy: Giant Corrugations of the Graphite Surface". *Phys. Rev. Lett.* **1986**, *57*, 3235.
35. Crommie, M. F.; Lutz, C. P.; Eigler, D. M. Confinement of Electrons to Quantum Corrals on a Metal Surface. *Science* **1993**, *262*, 218–220.
36. Heinrich, A. J.; Lutz, C. P.; Gupta, J. A.; Eigler, D. M. Molecule Cascades. *Science* **2002**, *298*, 1381–1387.
37. Horcas, I.; Fernandez, R.; Gomez-Rodriguez, J. M.; Colchero, J. WSXM: A Software for Scanning Probe Microscopy and a Tool for Nanotechnology. *Rev. Sci. Instrum.* **2007**, *78*, 013705.